

Transient Nonisothermal Fully Coupled Wellbore/Reservoir Model for Gas-Well Testing, Part 2: Applications

M. Bahonar, SPE, J. Azaiez, and Z. Chen, SPE, University of Calgary

Summary

After the development of a numerical fully implicit nonisothermal wellbore/reservoir simulator in Part 1 of this study (Bahonar et al. 2010), this simulator is implemented for a close and detailed study of gas-well pressure-drawdown (DD) and -buildup (BU) tests. Overall, the developed simulator is an accurate and strong tool for design and analysis of transient gas-well testing, particularly for high-pressure/high-temperature (HP/HT) gas reservoirs.

Several numerical results will be presented. This includes demonstration of the behaviour of the wellbore-fluid pressure, temperature, density, and velocity and an overall heat-transfer coefficient during DD or shut-in tests for nonisothermal reservoirs and conceptual comparisons with the isothermal counterparts. Thermal effects on the behaviour of derivative plots and the sandface-flow rate of deep nonisothermal gas reservoirs will be studied. A significant effect of neglecting the heat capacity of tubular and cement materials on the wellhead-temperature simulation, and thus transient well tests, will be demonstrated. A sample case to show that neglecting the thermal effects in the gas-well tests of composite reservoirs leads to unreliable results in well-testing analysis will be presented. Several other numerical experiments, including the presence of a variable wellbore-storage coefficient, gas backflow from the wellbore to the reservoir, and other thermal effects during the gas-well tests, are also presented.

Hundreds of millions of dollars are spent every year on well testing around the world (Hawkes et al. 2001). A proper design and truthful interpretation of these tests can be achieved by a reliable coupled wellbore/reservoir simulator, which in turn can save a large portion of the required costs.

Introduction

Well testing is one of the tools used in the petroleum industry that estimates reservoir properties (e.g., permeability, skin factor, average reservoir pressure, and effective reservoir compressibility) and reservoir characteristics (e.g., distance to a fault, naturally fractured or hydraulically fractured properties). During the test, a flowing well with a constant-flow rate is shut in or an already shut-in well is allowed to flow with a constant rate. During these periods of time, the transient pressure responses vs. time are recorded—preferably near the sandface or at any depth of the well if it is not possible—and then are analyzed. A basic assumption behind any well testing is that data are recorded directly from the reservoir, but in reality these data are always measured within the wellbore. Although solely measuring the reservoir responses is the desire of a well test, unfortunately the wellbore responses are also gathered by pressure recorders because they are employed within the wellbore and not within the reservoir. Another reason that the recorders are much more sensitive to the wellbore responses than to the reservoir responses results from the nature of phenomena that are happening in the wellbore and reservoir; the wellbore fluid has infinite transmissivity, whereas the reservoir flow is diffusive and thus slower than the wellbore counterpart.

In brief, the quality of data and analyzed results from a well test is confined to two important issues.

First, nonreservoir phenomena, particularly wellbore dynamics, quite often distort or even mask reservoir data. Therefore, these data may become useless or result in misdiagnosis, and most of the time they are difficult to interpret. Two examples of such phenomena are associated with wellbore storage (Agarwal et al. 1970) and phase redistribution (Fair 1981). Some other wellbore dynamics that can easily be misinterpreted as complex reservoir characteristics were reported by Mattar and Santo (1992), which included liquid influx/efflux, wellbore cleanup, plugging, recorder effects, and mysterious effects. However, they did not present the temperature effects on the wellbore fluids and transient tests. In fact, one of their basic assumptions behind the pressure-transient analysis was that the temperature was constant inside the reservoir and wellbore. Nevertheless, temperature effects on the well test have been seen in the field (Fan et al. 1999; Hawkes et al. 2001) and studied by some investigators (Kabir et al. 1996; Fan et al. 2000; Hasan et al. 2005; Izgec et al. 2007) by developing a variety of coupled wellbore/reservoir simulators. Some of the similarities and differences between these simulators and some of their drawbacks and advantages, have been described in Part 1 of this research study (Bahonar et al. 2010), in which these simulators have also been compared with our developed simulator. This new simulator will be used in the current paper to investigate thermal effects on transient pressure tests. Fan et al. (2000) studied only thermal effects for pressure-BU tests because of some assumptions used in their model. They also presented a conventional gas reservoir that may be misdiagnosed as a dual-porosity reservoir because of its thermal effects. In contrast to the work of Fan et al. (2000), we investigate the thermal effects for both flowing and shut-in tests and present a new sample case in which the true reservoir characteristics can be easily misinterpreted by analytical models as a result of temperature effects. Additionally, we present the behaviour of the wellbore-storage coefficient with respect to time in both DD and BU tests. Moreover, we compare this coefficient between numerical isothermal and nonisothermal models and analytical models in a way that is more clear compared with previous works. Other numerical experiments that have not received much attention before will also be presented.

The second issue that limits the quality of data and analyzed results from a well test is related to technological tools that make the well-testing process more difficult or even impossible compared with ideal well-testing operations. The ideal cases are those in which the tools are placed right alongside the sandface and isolated from the casing by packers to minimize the wellbore storage and other effects. In these ideal cases, the well-testing costs are also affordable. However, in reality, well-testing jobs are not simple and straightforward in some reservoirs (e.g., exceptionally deep HP/HT gas reservoirs) where failure of well-testing tools is common. The situation becomes even more difficult if the flowing fluid from the reservoir contains sour and corrosive gases (e.g., carbon dioxide and/or hydrogen sulphide). In this type of reservoir, even if we can run the well-testing tools, the process will be quite difficult and costly. Furthermore, the acquired data will be unreliable (Wang 1996). A possible remedy is to install permanent pressure and/or

**TABLE 1—INPUT PARAMETERS FOR THE BASE CASE
OF DEVELOPED NONISOTHERMAL MODEL**

Default wellhead constraint (rate or pressure)	constant gas prod. rate
Reservoir permeability (md)	1
Reservoir porosity (fraction)	0.10
Connate water saturation (fraction)	0.20
Water compressibility (psia ⁻¹)	1.0 E-06
Gas-production rate (MMscf/D)	5.0
Gas-specific gravity (80% methane and 20% ethane)	0.651
Gas-critical pressure (psia)	675.43
Gas-critical temperature (°F)	384.41
Gas density at standard conditions (lbm/scf)	0.049845
Geothermal gradient (°F/ft)	0.0165
Number of reservoir grids	20
Net pay thickness (ft)	30
Reservoir area (acre)	100
Reservoir pressure gradient (psi/ft)	0.6
Rock compressibility (psia ⁻¹)	1.0 E-06
Skin factor	0
Total depth of the well (ft)	15,000
Wellhead minimum pressure for switching well constraint (psia)	200
Wellbore radius (ft)	0.667
Surface temperature (°F)	70
Standard condition for pressure (psia)	14.696
Standard condition for temperature (°F)	60
Reference pressure for porosity (psia)	14.7
Wellbore segment length (ft)	200
Wellbore segment roughness (ft)	0.000018
Wellbore segment inclination (degree)	0
Annulus pressure at wellhead (psia)	14.7
Number of formation (earth) grids in radial direction	5
Inside radius of tubing (ft)	0.106167
Outside radius of tubing (ft)	0.145833
Inside radius of casing (ft)	0.375000
Outside radius of casing (ft)	0.447917
Formation (earth) external radius (ft)	500
Emissivity of casing inside surface (dimensionless)	0.9
Emissivity of tubing outside surface (dimensionless)	0.9
Thermal conductivity of tubing [Btu/(sec ft °F)]	0.006944
Thermal conductivity of casing [Btu/(sec ft °F)]	0.006944
Thermal conductivity of cementing [Btu/(sec ft °F)]	0.000320
Thermal conductivity of formation in radial direction [Btu/(sec ft °F)]	0.000556
Thermal conductivity of formation in axial direction [Btu/(sec ft °F)]	0.000556
Formation density (lbm/ft ³)	187.2
Formation heat capacity [Btu/(lbm °F)]	0.186779
Formation thermal diffusivity (ft ² /sec)	1.590160 E-05
Thermal resistance skin factor	0
Thermal storage parameter	0
Maximum timestep (sec)	1,000
Minimum timestep (sec)	1
Producing time duration (sec)	200,000
Shut-in time duration (sec)	200,000
Timestep at the start of production or shut-in (sec)	1
Tolerance	1.0 E-06

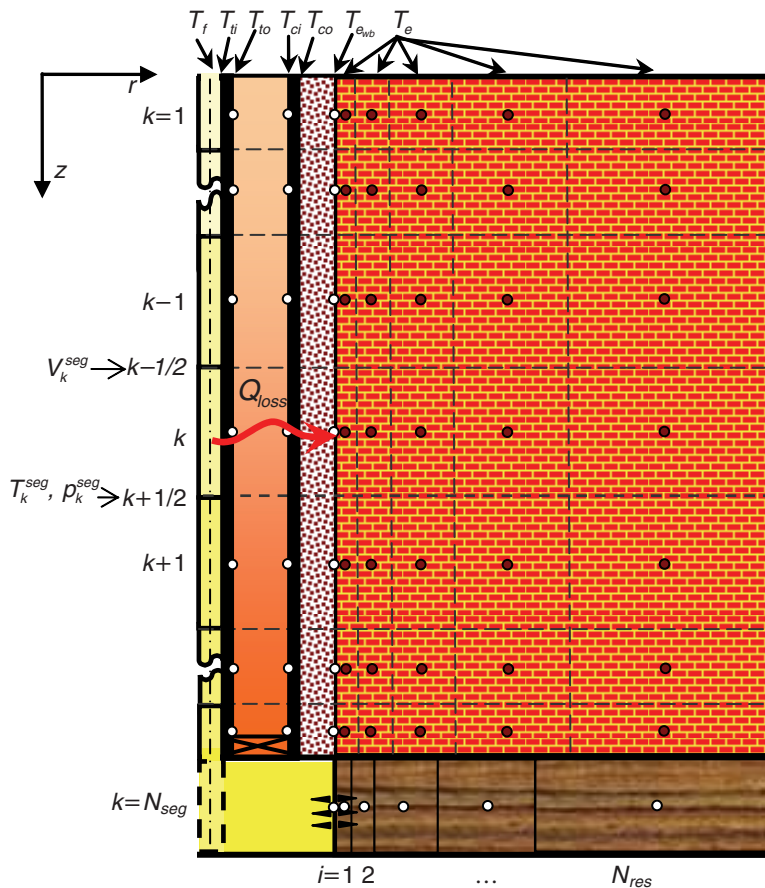


Fig. 1—Schematic of the discretized reservoir, wellbore, and formation (earth).

temperature recorders at the bottomhole and shut in the well at the wellhead rather than at the bottomhole by means of a downhole shut-in valve. Therefore, the well test becomes more economical and can be performed as many times as desired. The gathered pressure data may be analyzed to describe the reservoir characteristics. However, in this case, great care must be taken in respect to the data because wellbore dynamics and thermal effects, particularly in HP/HT reservoirs, often distort reservoir data and consequently reservoir characteristics may be misdiagnosed. To avoid this pitfall, coupled wellbore/reservoir simulators [e.g., the one developed in Part 1 of this study (Bahonar et al. 2010)] can be employed. In the current work, our base case for all studies will be in fact an HP/HT reservoir with the presence of wellbore dynamics.

In the next section, we first define a base-case and then change one or a few parameters at a time to study some reservoir and/or wellbore behaviours. The results of this study will help analysts to more accurately interpret the pressure-transient data for both isothermal and nonisothermal reservoirs, and the developed simulator in Part 1 of this study (Bahonar et al. 2010) will help engineers to more effectively design well tests in terms of, for example, time and costs.

Results and Discussions

The reservoir, wellbore, well-completion, and formation data along with gas properties that are used in this study are typical data obtained along the US Gulf of Mexico coast (Fan et al. 2000) and are tabulated in **Table 1**. This information is used in the base-case study and with minor changes (often a parameter at a time except in the study of a composite reservoir) is used for other cases to investigate how the wellbore dynamics affects the transient pressure analysis. A schematic of the reservoir, wellbore, and formation is sketched in **Fig. 1**. For clarification, from now on in the legend of the figures and in the body of the paper, we refer to the numerical isothermal or nonisothermal simulator that has been developed in Part

1 of the study by “isothermal simulator” or “nonisothermal simulator,” respectively, while analytical models that are available in the commercially accessible well-testing software F.A.S.T. WellTest (2009) will be referred to as the “analytical models.” Therefore, well-testing software and the analytical models are interchangeable in meaning. Furthermore, Appendix A provides the definition of the terms and parameters that are used in the x - or y -axis of the figures. Results for the different scenarios are discussed next.

The Base Case. A DD with 5 MMscf/D wellhead gas-flow rate, followed by a shut-in at wellhead (i.e., BU test) for 55.56 hours each, is simulated by the input data presented in **Table 1**. The base case is designed in a way that we can see all the necessary flow periods, including the early time (momentum effect), significant wellbore-dynamics period (transition period or afterflow period), temperature-affected period, and true reservoir transient period (infinite-acting regime). For the composite-reservoir case (last case) that will be presented later, we increase the producing and shut-in time to also see the pseudosteady-state period and boundary effects. The gas reservoir has 15,000-ft depth, 1-md permeability, zero skin factor, 9,000 psia (the initial pressure), 317.5°F (the initial temperature), and 100 acres of area. **Fig. 2** shows the bottomhole pressure (BHP), average wellbore pressure, wellhead pressure (WHP), and the wellhead gas-flow rate vs. time. This indicates that the BHP reaches 6,134.6 psia (31.8% DD) at the end of the DD period. It can also be seen from this figure that the three pressure curves (BHP, average wellbore pressure, and WHP) are moving with the same trend with a nearly constant ordinate difference. This means that if the WHP data are analyzed directly, approximate reservoir properties can be still obtained. For example, we analyze the WHP in which approximately correct reservoir permeability is obtained (1.22 md from the DD and 1.12 md from the BU test). However, as a result of the ordinate difference previously mentioned, a large positive value for the skin

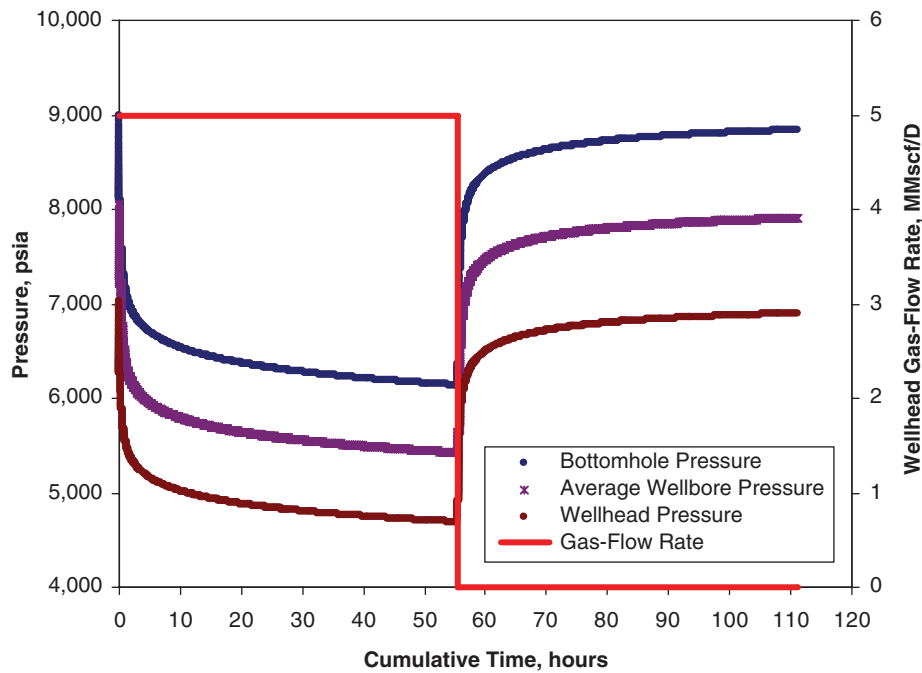


Fig. 2—BHP, average wellbore pressure, WHP, and wellhead gas-flow rate vs. time.

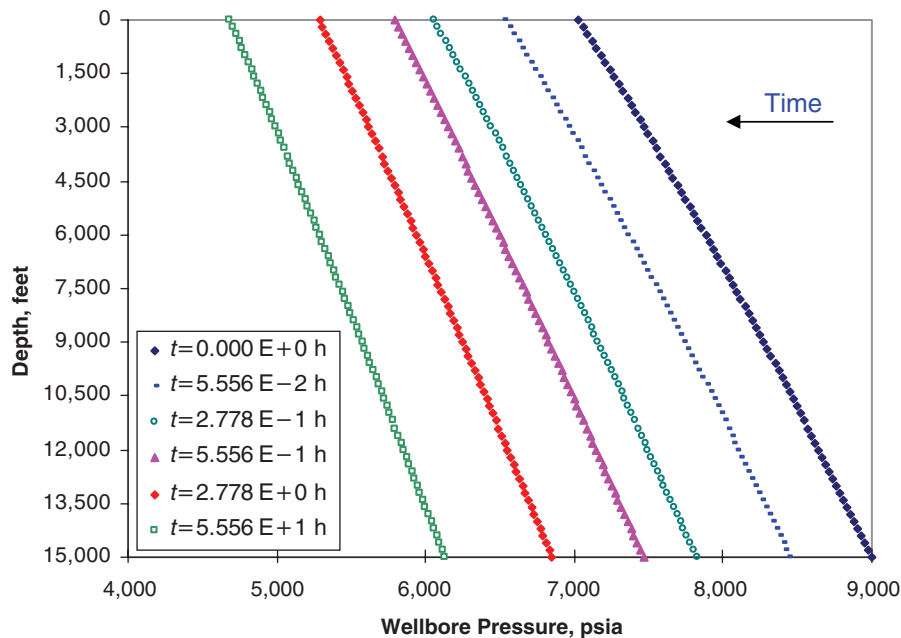


Fig. 3—Change of pressure profile along the wellbore with time (DD test).

factor (5.5) from the DD test and a small negative skin factor (-0.4) from the BU test are estimated in contrast with the zero skin factor of the reservoir. This error can be reduced simply by subtraction of the hydrostatic pressure from the WHP to translate it to the BHP in the case where the frictional pressure drop is negligible. Note that the quality of the WHP for the transient analysis drops substantially as the reservoir formation thickness and/or reservoir permeability increases (Hasan et al. 2005). For a large value of reservoir-flow capacity (permeability multiplied by the reservoir formation thickness), the transient analysis of the WHP becomes impossible.

Wellbore Profiles for the Base Case. Fig. 3 shows the pressure profile inside the wellbore during the DD period. As can be seen, the wellbore pressure drops almost linearly from its initial profile to the final one. The same linearly increasing trend can be seen from

Fig. 4 for the BU period. Fig. 5 indicates the increase in the wellbore temperature from its initial geothermal temperature (that was assumed to be linear) to the final temperature distribution at the end of the DD period. This increase is caused by the flow of the hot gas (317.5°F) from the reservoir through the wellbore. However, during the BU period the gas inside the wellbore loses its heat toward the colder formation and thus its temperature decreases, as illustrated by Fig. 6. Figs. 7 and 8 show the nonlinear time-dependent behaviour of the gas-density profile in the wellbore during the DD and BU periods, respectively. This nonlinearity and time dependency should be considered once it is intended to convert the WHP to the BHP. Fig. 7 indicates a decrease in the gas-density profile because of a warming of the wellbore during the DD, while Fig. 8 shows an increase in the gas density because of the cooling effect and pressure increase in the wellbore during the BU. This increase in the gas density can be

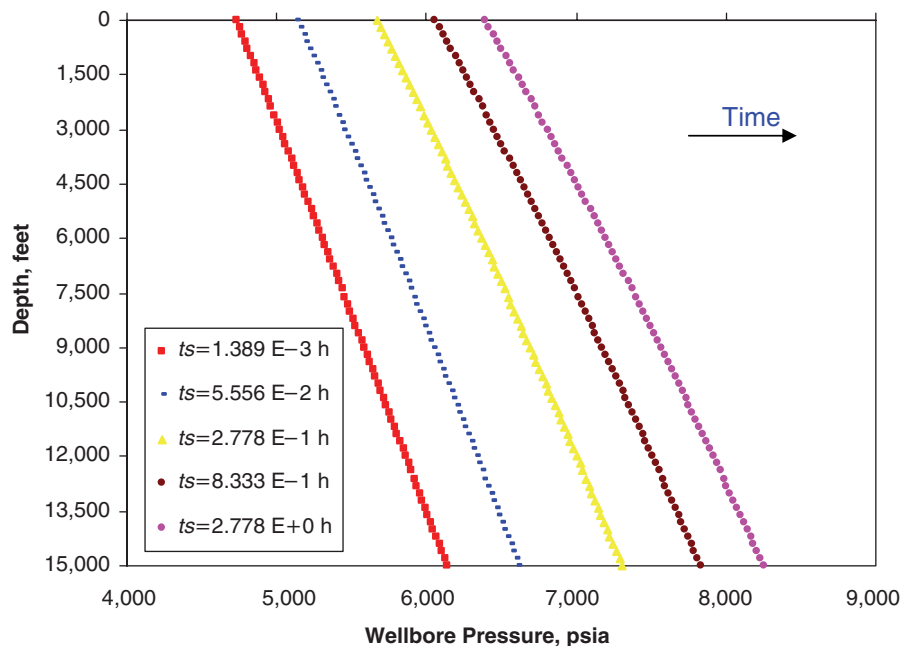


Fig. 4—Change of pressure profile along the wellbore with time (BU test).

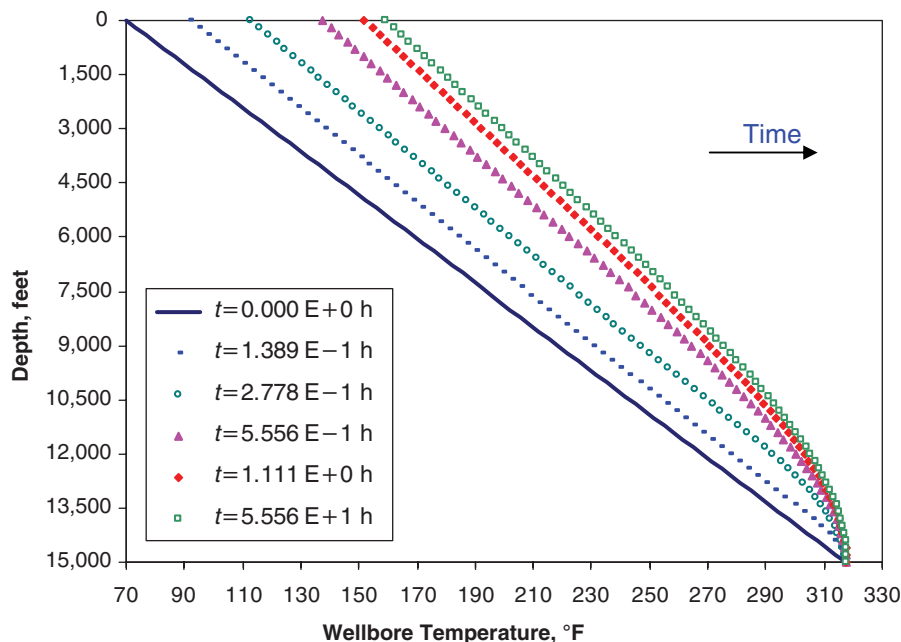


Fig. 5—Change of temperature profile along the wellbore with time (DD test).

explained by exploring the temperature (Fig. 6) and pressure (Fig. 4) profiles during the BU period. If we only had temperature effects, the density profiles would become similar to the temperature profiles with nearly a constant density at the bottomhole condition where the temperature is also nearly constant (Fig. 6). However, the pressure increase is approximately 2,000 psia everywhere along the wellbore during the BU, which significantly increases the density everywhere, including the bottomhole. This is the reason that even though the temperature profiles start from a single point at the bottomhole, the density profiles spread over the x -axis as with the pressure profiles. Fig. 8 also indicates that at early time in the BU period, the behaviour of the density profiles is relatively nonlinear, but as the tubing-fluid pressure and temperature change, decrease, and reach equilibrium at a later time, the behaviour of the density profiles becomes more linear. Both figures show that the denser fluid resides near the wellhead compared with the bottomhole, which is caused by the lower

temperature at the wellhead compared with the bottomhole. Note that because of a higher pressure at the bottomhole compared with the wellhead, we may expect that the denser fluid should be at the bottomhole. Because of larger temperature effects compared with those of pressure, an opposite result occurs. **Fig. 9** indicates the increase in the gas-velocity profile in the wellbore during the DD. Note that at early times, most of the fluid is produced from the wellbore, not from the reservoir. This explains why after 5 seconds, the velocity at the bottomhole is 0.23 ft/sec while it is 3.75 ft/sec at the wellhead (Fig. 9). However, as Fig. 9 shows, after approximately 0.278 hours (1,000 seconds), the reservoir mostly feeds the wellbore and velocity at both the wellhead and bottomhole, which reaches approximately 4 ft/sec. As the wellhead-flow rate was set to zero in the BU period, the gas-velocity profile continuously decreases to approach zero, as illustrated by **Fig. 10**. Yet, after 2.78 hours (10,000 seconds) a small gas velocity of 0.04 ft/sec can be traced particularly near the bottomhole.

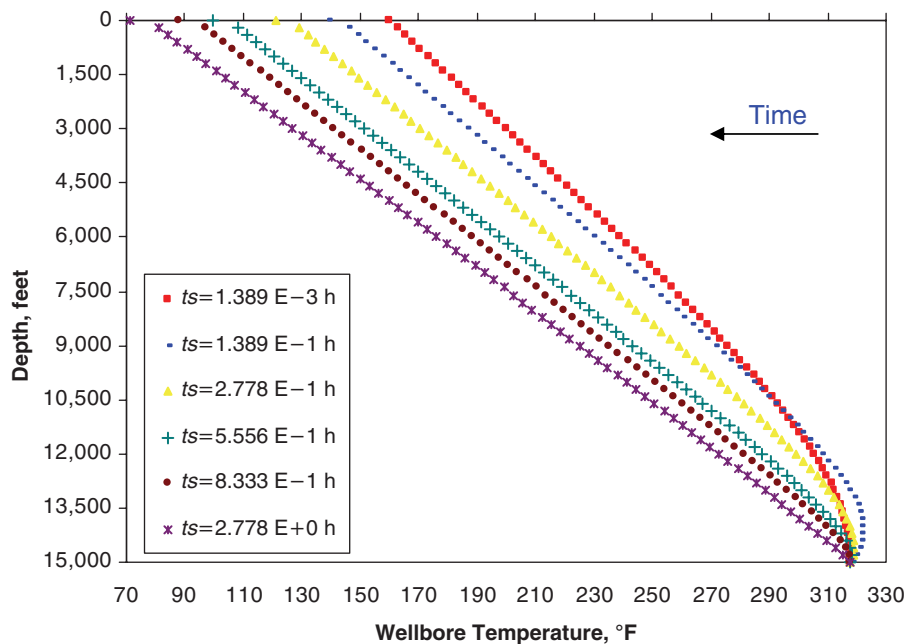


Fig. 6—Change of temperature profile along the wellbore with time (BU test).

One of the important parameters that affect the solution of the whole system is the heat-loss estimation, which connects the energy equation inside the wellbore to the heat-transfer equation in the formation. Heat loss is a function of the difference between the fluid temperature inside the tubing and the wellbore temperature, and an overall heat-transfer coefficient. This coefficient is a non-linear function of several heat resistances from the tubing to the cement/formation interface. These heat resistances include the heat conduction in the tubing, casing, and cement, and the heat conduction, natural convection, and thermal radiation inside the wellbore annulus. The heat conduction, natural convection, and thermal radiation are calculated on the basis of the thermal conductivity of the stated materials, a correlation that is a function of the Grashof number, the Prandtl number, and the Stefan-Boltzmann law, respectively (Bahonar et al. 2011a, b). As the depth of the wellbore annulus increases, the annulus temperature and pressure increase as a result of an increase in the geothermal temperature and gas hydrostatic column inside the annulus, respectively. These factors boost the thermal radiation and natural convection inside the wellbore annulus and result in an increase in the overall heat-transfer coefficient as a function of depth. As time elapses, the overall heat-transfer coefficient increases during the DD because the wellbore annulus warms up as a result of the hot gas production (Fig. 11). During the BU period, however, as a result of heat loss, the annulus temperature drops and consequently the overall heat-transfer coefficient decreases, as shown by Fig. 12. Therefore, in general, the overall heat-transfer coefficient is a nonlinear transient depth- and temperature-dependent parameter that should be modelled properly.

Because most of the fluid properties are strong functions of a temperature change, most of the nonlinearities in different profiles emerge as a result of nonlinearity in the temperature profile (Figs. 5 and 6). Therefore, the profiles of wellbore variables for the isothermal case become quite simple because there is no temperature change and thus will not be presented here.

Derivative Curves for the Base Case. Figs. 13 and 14 compare the derivative plots for the DD and BU tests, respectively, for three cases of numerical isothermal and nonisothermal models, and analytical models. According to Figs. 13 and 14, the deviations among these three models occur in the middle time, which is caused by the sandface-flow rate (the afterflow rate in the case of the BU test) and temperature effects. The analytical models that assume the wellbore-storage coefficient is constant (the validity of this as-

sumption will be clearly judged subsequently) show the narrowest humps. These models cannot model the temperature effects. Then, we have a prediction of the isothermal model that has wider humps compared with the analytical models as a result of accurate modelling of the wellbore-storage phenomenon in the well that is opened or shut-in at the wellhead. As can be seen from Figs. 13 and 14, as a result of a higher wellbore-storage coefficient in the isothermal model compared with the analytical models, the transient radial-flow period will be seen at a later time. Last, we have the nonisothermal model with the widest and most deformed humps, compared with both the isothermal and analytical models, because of temperature effects. In fact, in nonisothermal gas reservoirs, the reservoir responses are even more masked compared with those of isothermal gas reservoirs in consequence of an increase in the wellbore-storage coefficient by thermal effects. The behaviour of the wellbore-storage coefficient of the three stated models for both DD and BU periods will be presented next.

Sandface-Flow Rates for the Base Case. Figs. 15 and 16 show the sandface-flow rate and afterflow rate for the DD and BU periods, respectively, for both the isothermal and nonisothermal models. They also show the change of the wellhead temperature during the tests. Fig. 15 indicates that in the nonisothermal case the sandface-flow rate reaches 99% of the wellhead-flow rate, which is 4.95 MMscf/D after 2.25 hours, while in the isothermal case the sandface-flow rate reaches 99% of the wellhead-flow rate after 1.93 hours (19 minutes earlier). Fig. 16 shows that the afterflow rate reaches 0.05 MMscf/D (close to the wellhead-shut-in-flow rate, which is zero) after 2.35 hours shut-in time in the nonisothermal case and after 1.71 hours shut-in time (38 minutes earlier) in the isothermal case. The differences between the two plots at the middle time in both graphs result from the temperature effects on the wellbore-storage phenomenon. This temperature effect emerges as a result of hot-gas convection inside the tubing and heat loss from the tubing fluid toward the surrounding medium. Note that in the DD period, the forced-heat convection is dominant, whereas after some time the heat loss to the surrounding cold medium is the dominant heat-transfer mechanism in the BU period.

Wellbore-Storage Coefficient for the Base Case. As stated in the Introduction, one of the important factors that affects the transient pressure behaviour and may cause an incorrect estimation of reservoir properties is the wellbore-storage effect. This effect occurs

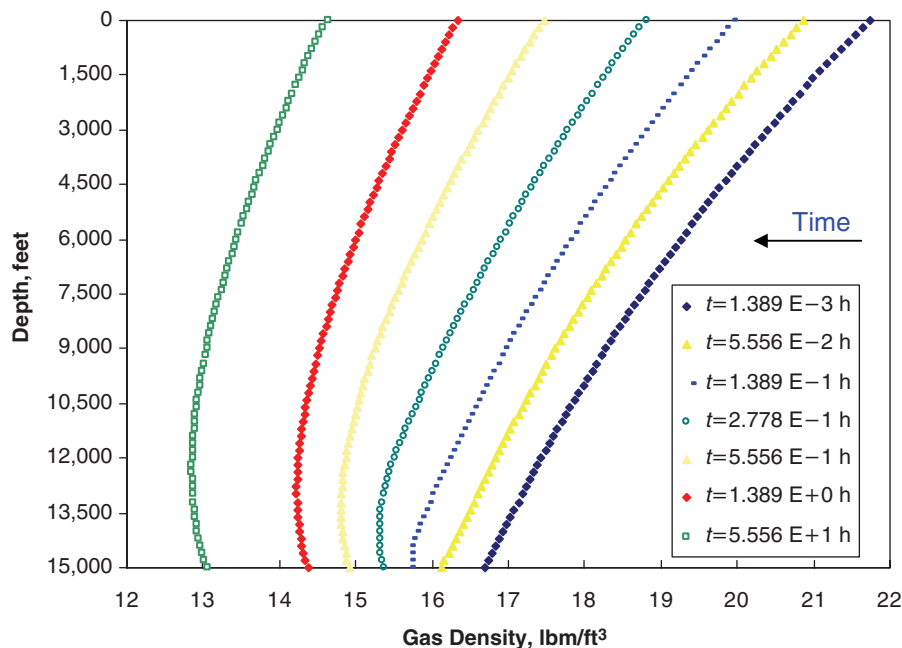


Fig. 7—Change of gas-density profile along the wellbore with time (DD test).

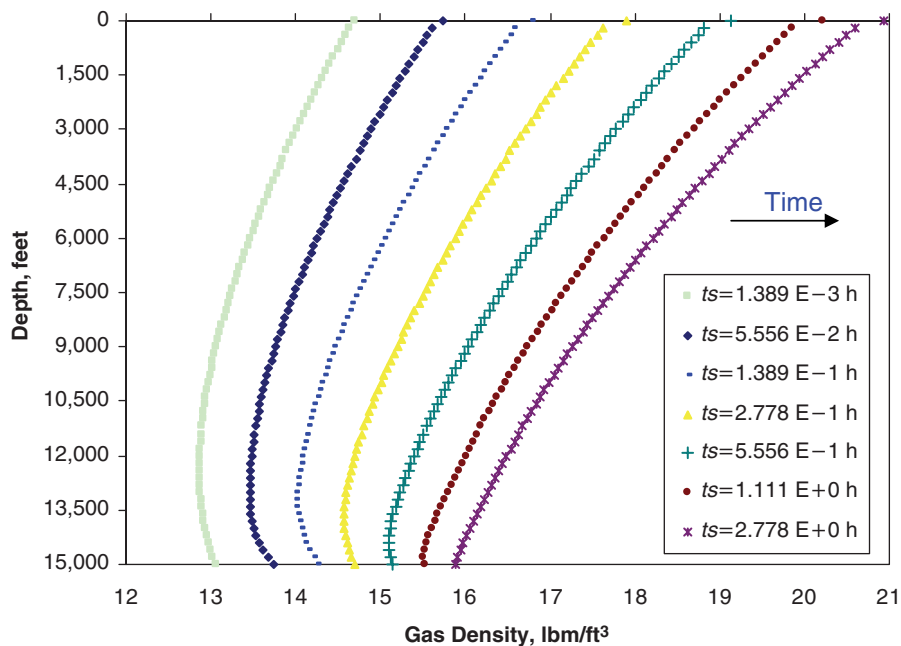


Fig. 8—Change of gas-density profile along the wellbore with time (BU test).

as a result of fluid expansion in the wellbore during the DD period and because of afterflow from the reservoir to the wellbore during the BU period, even after the well has been shut in. To model this phenomenon, a parameter known as the wellbore-storage coefficient is defined in well testing and is equal to the change in the total volume of wellbore fluids per unit change in the BHP. It is usually reported in units of bbl/psia or is nondimensionalized. For simplicity, in most well-testing software and analytical models, this parameter is often assumed to be constant. In this case, for a completely gas-filled wellbore it will be equal to the product of the wellbore volume and the wellbore-gas compressibility. However, the assumption of a constant wellbore-storage coefficient is not often correct in the field (Meunier et al. 1985). In some cases, the influence of changing wellbore storage on the well test may be so severe that the data obtained from it may be difficult to analyze or

even impossible to analyze. Therefore, it is important to estimate the duration of influence of the wellbore-storage effect on the transient pressure data. This estimated time, particularly for the nonisothermal wellbore/reservoir systems, can be obtained by running an appropriate simulator that helps to design a well test with enough time to acquire good-quality data not distorted by the wellbore effects. We employ the equations of a variable wellbore-storage coefficient (Sabet 1991) for the DD and BU tests given by Eqs. 1 and 2, respectively, for both the numerical isothermal and nonisothermal simulators to study the behaviour of this wellbore-storage coefficient as time elapses:

$$C(t) = \frac{(q_{sf} - q_{wh})_{sc} B_g}{dp_{wf}/dt} \dots\dots\dots (1)$$

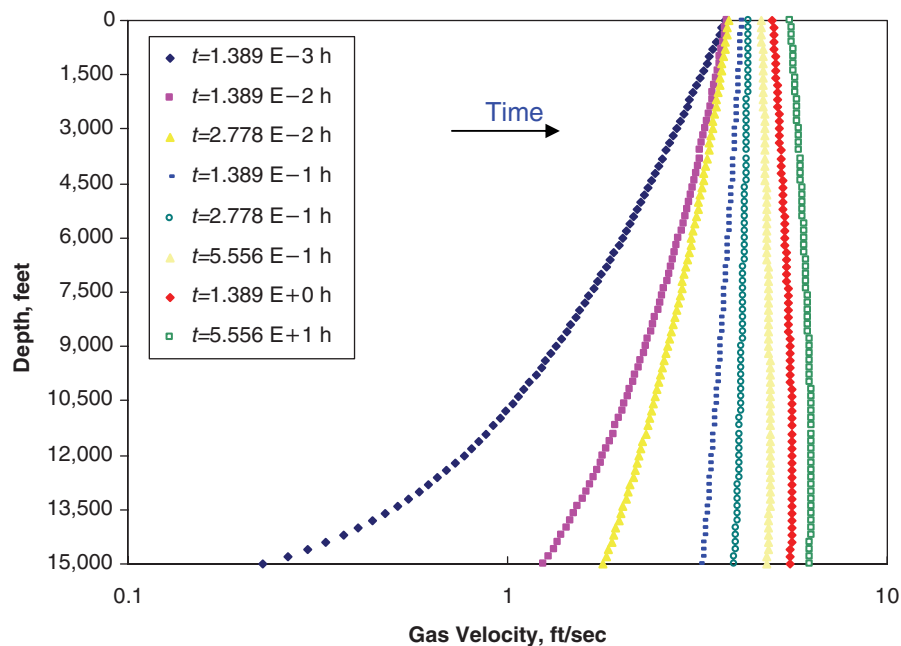


Fig. 9—Change of gas-velocity profile along the wellbore with time (DD test).

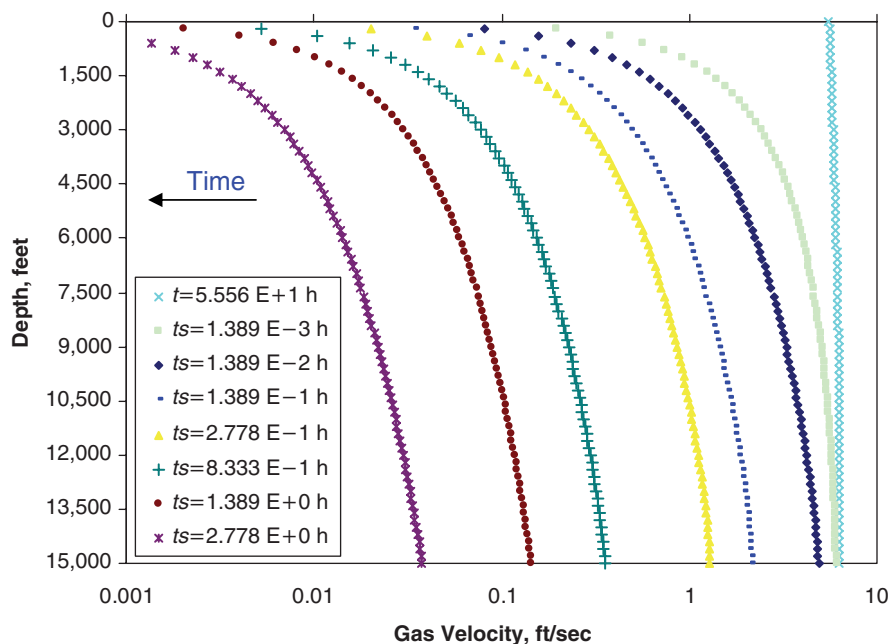


Fig. 10—Change of gas-velocity profile along the wellbore with time (BU test).

$$C(t) = \frac{(q_{sf})_{sc} B_g}{dp_{ws}/dt} \quad (2)$$

In Eqs. 1 and 2, B_g is calculated at the BHP and temperature. **Figs. 17 and 18** show the change of the wellbore-storage coefficient vs. time for the DD and BU periods, respectively. Fig. 17 demonstrates that for the nonisothermal DD period, the wellbore-storage coefficient is clearly not constant and changes significantly from 0.02 to 2 hours. In contrast, for the isothermal case, we can see a mild increase in the wellbore-storage coefficient because of an increase in the gas compressibility as a result of the pressure DD. This increase is small, and the wellbore-storage coefficient can

be averaged over the whole period of time and assumed to be constant. If the transient BHP that is generated by our simulator is interpreted by the well-testing software, it gives a constant value for the wellbore-storage coefficient that has been plotted in the same figure. This value is close to the variable wellbore-storage coefficient that is calculated from the isothermal simulator, as shown in Fig. 17. The same observation as previously mentioned for the DD period (Fig. 17) is true for the BU period (Fig. 18), except that the wellbore-storage coefficient is decreasing in this case as a result of a decrease in the wellbore-gas compressibility. Note that the time period in which significant changes happen in the wellbore-storage coefficient of the nonisothermal DD and BU tests (the humps in Figs. 17 and 18) coincides with the time period in which discrepancies appear in the plots of derivatives and sandface flow curves (Figs. 13 and 14, and Figs. 15 and 16, respectively) between the

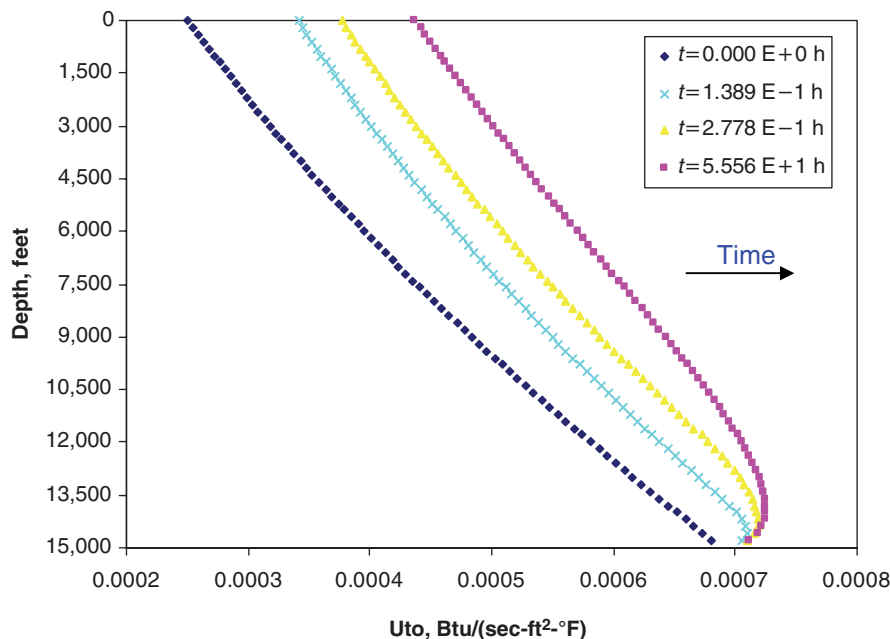


Fig. 11—Change of overall heat-transfer-coefficient profile along the wellbore with time (DD test).

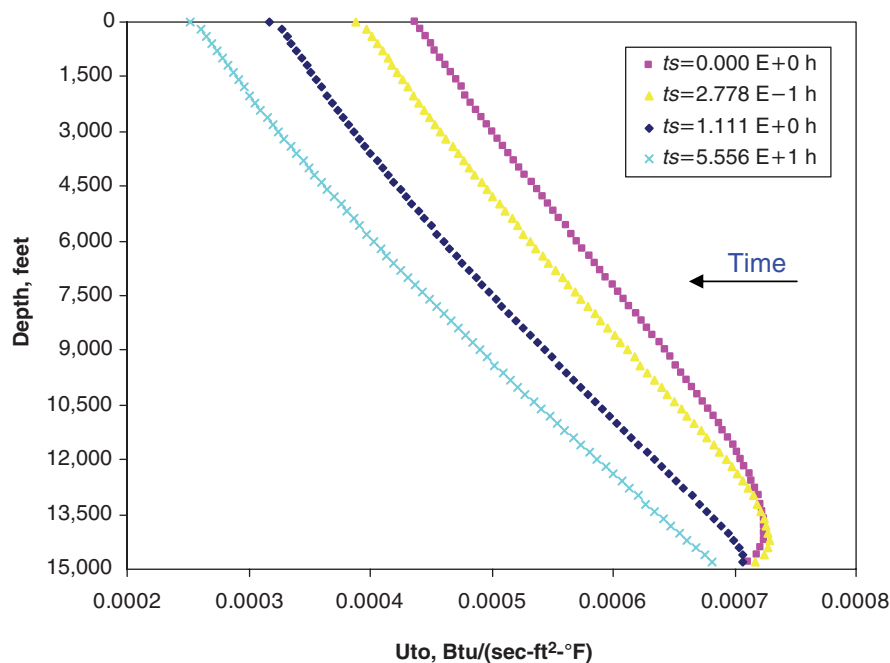


Fig. 12—Change of overall heat-transfer-coefficient profile along the wellbore with time (BU test).

nonisothermal and isothermal cases. The true transient time will start at the time at which the humps disappear in Figs. 17 and 18. Therefore, these graphs can be readily used to design the time of tests to be long enough to acquire data not distorted by the wellbore dynamics.

In the first portion of Figs. 17 and 18, the wellbore-storage coefficients for both isothermal and nonisothermal cases show a sharp drop because of the momentum effect. This behaviour can be explained by looking at Eqs. 1 and 2. On the basis of these equations at early time of the wellbore opening or shut-in, the numerators of these equations have a certain defined value, but the denominators are zero until the perturbation at the surface as a result of the valve opening or closing reaches the bottomhole. Until that time, the values of these equations are infinite, but dramatically drop from a large number to a defined number after a few seconds.

In the last time segment of Fig. 18, the wellbore-storage coefficient starts to rise as a result of small values of the numerator and denominator in Eq. 2. In other words, at a larger time during the BU test, both the sandface-gas-flow rate (numerator) and the changing of shut-in pressure with respect to time (denominator) approach zero. Also, note that in the field, a bottomhole flowmeter has a threshold that cannot measure the flow rate below a certain value (e.g., 0.01 ft³/sec).

To summarize, the wellbore-storage coefficient not only changes with respect to time, but is also largely affected by nonisothermal effects.

Thermal-Storage Parameter Case. In the modelling of the nonisothermal coupled wellbore/reservoir simulator (Bahonar et al. 2010), the heat accumulation for the tubular and cement materials was ne-

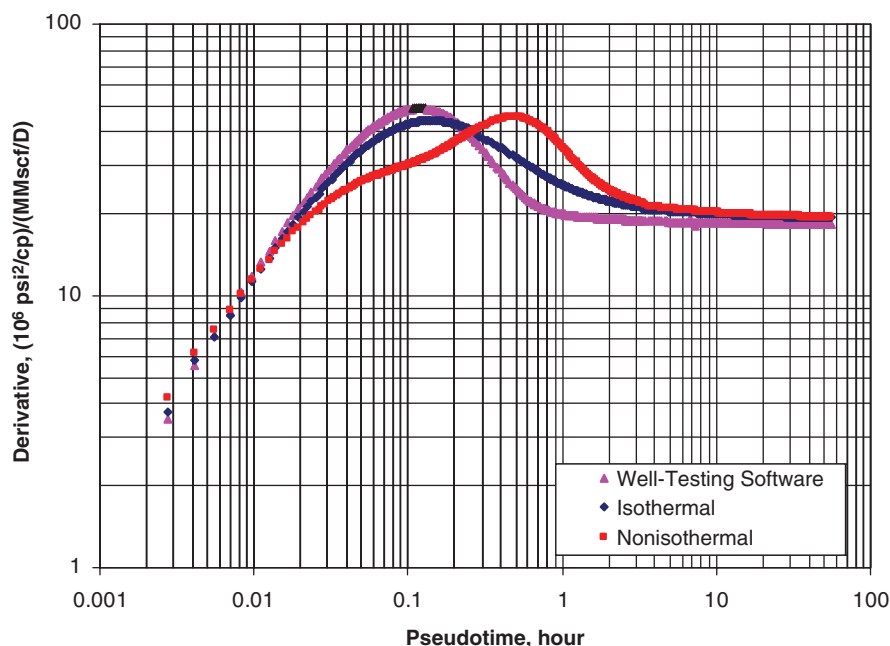


Fig. 13—Comparison of derivative curves for numerical isothermal and nonisothermal models, and analytical models (DD test).

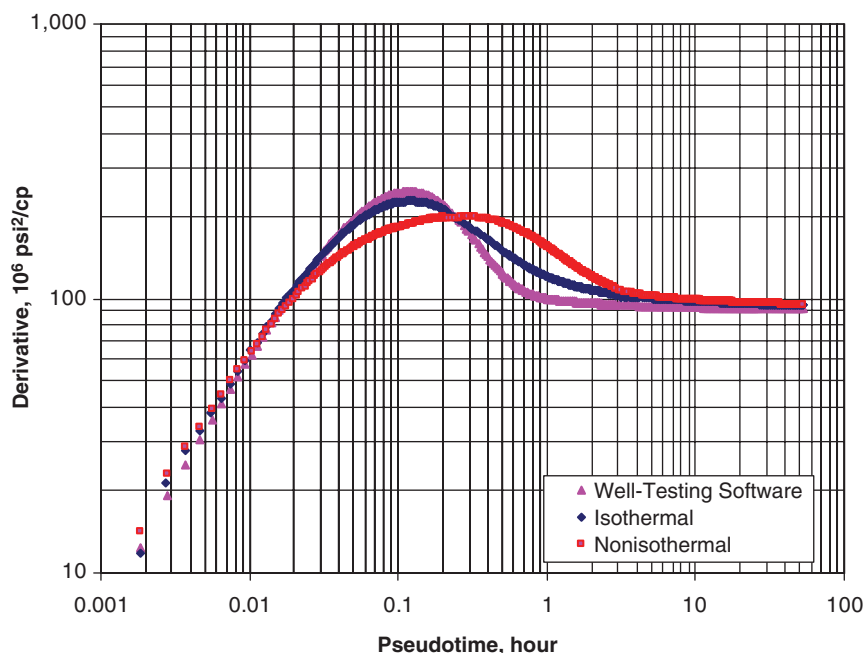


Fig. 14—Comparison of derivative curves for numerical isothermal and nonisothermal models, and analytical models (BU test).

glected. This means that any heat lost from the tubing fluid is not absorbed by these materials and directly transfers to the formation. The reason for this assumption was that the annulus is a nonporous medium and thus needs computational-fluid-dynamics (CFD) techniques to model it. However, the annulus extends some thousands of feet deep and hence its modelling even with the CFD techniques is nearly impossible at the moment. But we know that at the initial DD or BU period, these materials will accumulate some heat and affect the transient data. To remove this pitfall, the accumulation term in the energy-balance equation of the wellbore fluid is multiplied by a coefficient $(1 + C_T)$, where C_T is called the thermal-storage parameter. This parameter indicates that the unsteady-state heat accumulation in the tubular and cement material is a fraction of the unsteady-state heat accumulation inside the wellbore. $C_T = 0$ corresponds to no accumulation in the tubular and cement material, while $C_T = -1$

results in neglecting the accumulation term for the fluid inside the tubing. The concept of the thermal-storage parameter was initially introduced by Hasan and Kabir (2002), and in a subsequent paper, they showed that a thermal-storage parameter value of 3.0 for DD and 2.0 for BU tests worked for their field tests (Hasan et al. 2005). Figs. 19 and 20 show how the wellhead temperature is affected by selecting different thermal-storage parameters for the DD and BU tests, respectively. It can be seen that different values of this parameter affect the plots in the first 2 and 10 hours of the DD and BU periods, respectively. After 2 hours of gas production, because the tubular and cement materials have already warmed up, the thermal-storage parameter has no effect on the wellhead temperature. Fig. 19 indicates that as this parameter increases, the wellhead temperature reaches a certain value at a later time because a higher heat capacity of these materials absorbs the energy of the tubing fluid. A larger

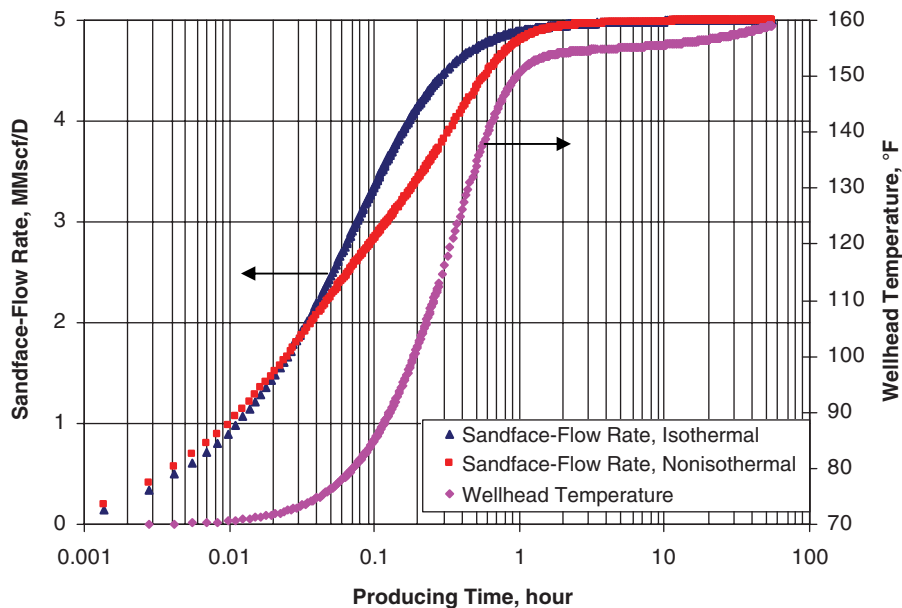


Fig. 15—Comparison of sandface-flow rate for numerical isothermal and nonisothermal models (DD test).

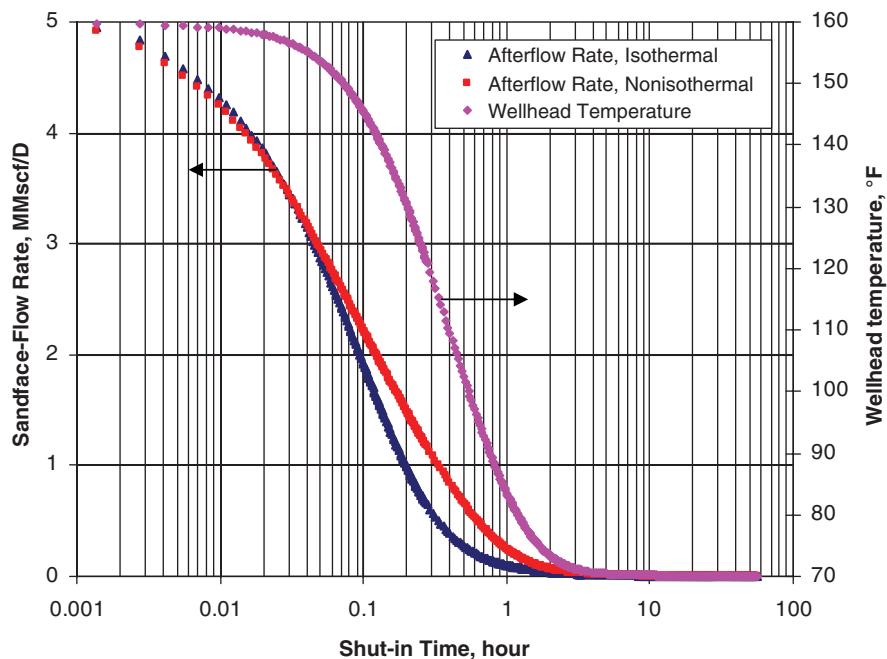


Fig. 16—Comparison of afterflow rate for numerical isothermal and nonisothermal models (BU test).

thermal-storage parameter against fast cooling during the BU and, therefore, the wellhead temperature reaches a certain value at a later time, as illustrated by Fig. 20.

Permeability Case. To investigate the effect of permeability on the transient pressure tests, different values of permeability, including 1, 10, 100, and 1,000 md, are used, which result in BHP of 6,135; 8,660; 8,961; and 8,996 psia at the instant of shut in. These pressure drops led to 31.83, 3.78, 0.43, and 0.04%-pressure DDs, respectively, compared with an initial reservoir pressure of 9,000 psia. To compare all curves in a single graph, we multiply the derivative values by the reservoir permeability. Figs. 21 and 22 show a strange behaviour of these modified-derivative curves for nonisothermal systems, particularly for high-permeability cases for the DD and BU tests, respectively. Fluctuations of derivative curves for the high-permeability values within the period of 0.02 hours are because of a fast response of these cases with respect to the pres-

sure change (large momentum effect). These fluctuations can easily result in the misdiagnosis of these systems. For instance, a combination of multilayer, composite, and/or dual-porosity systems can perfectly match such data; however, in this example we know that our reservoir is a conventional homogeneous single-layer system. Therefore, the well-testing analyst should be aware of these effects to prevent an incorrect interpretation. The momentum-dominated period, however, disappears quickly as a result of frictional loss (Fan et al. 2000). The afterflow period lasts for a few hours, and finally the true transient period will emerge. Note that for low-permeability cases that have a higher DD pressure and thus higher gas compressibility at the instant of shut-in, the significance of the momentum effect is less than for high-permeability cases. To understand this behaviour more clearly, Figs. 23 and 24 depict the afterflow rates for the numerical isothermal and nonisothermal simulators, respectively, for a variety of permeability values. In the isothermal case, Fig. 23 indicates that for the high-permeability cases

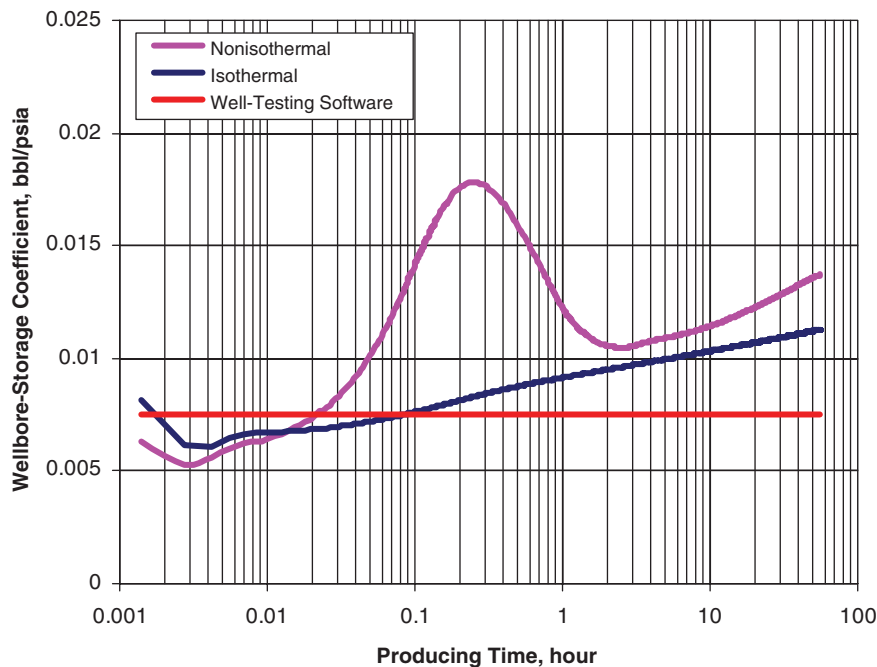


Fig. 17—Comparison of wellbore-storage coefficient for numerical isothermal and nonisothermal models, and analytical models (DD test).

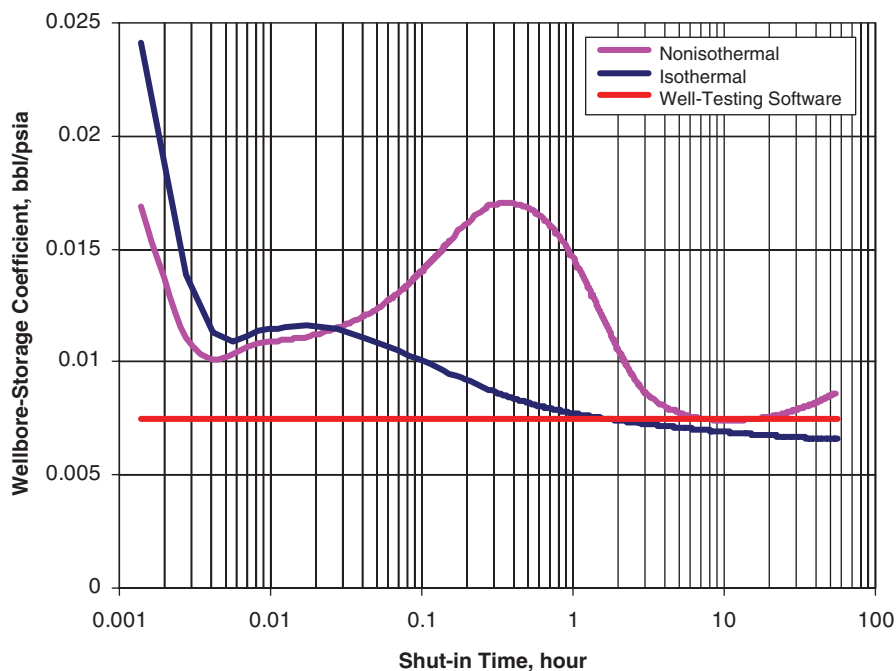


Fig. 18—Comparison of wellbore-storage coefficient for numerical isothermal and nonisothermal models, and analytical models (BU test).

(100 and 1,000 md), the afterflow rates show some fluctuations until they stop flowing; however, for the low-permeability cases, the direction of the afterflow rates never changes. For instance, for the 1,000-md case, as a result of a high momentum effect and sudden gas compression in the wellbore, the wellbore pressure temporarily increases dramatically, which results in the change in the flow direction. At this instant, gas flows at a high flow rate of approximately 20 scf/sec from the wellbore toward the reservoir. Following a few other fluctuations, the afterflow rate quickly dampens after 0.03 hours. For the nonisothermal cases (Fig. 24), the observation is a bit different. For the 1,000-md case, only one flow-direction change with a small negative flow rate can be seen, and for the 100-

md case, no flow-direction change can be identified compared with the isothermal case. Also, for the 1,000-md case, the afterflow rate lasts more than 2.5 hours compared with the isothermal case with only 0.03 hours of afterflow after well shut-in. Comparing Figs. 23 and 24, it can be concluded that the temperature effects enhance the afterflow rate and thus increase the wellbore-storage effects in the nonisothermal cases compared with the isothermal cases.

Tubing-Internal-Radius Case. Four different tubing internal radii are chosen to study its effect on the behaviour of derivative curves. We reduce the tubing internal radius of the base case by 33 and 50% in two cases and increase by 20% in another case. The pres-

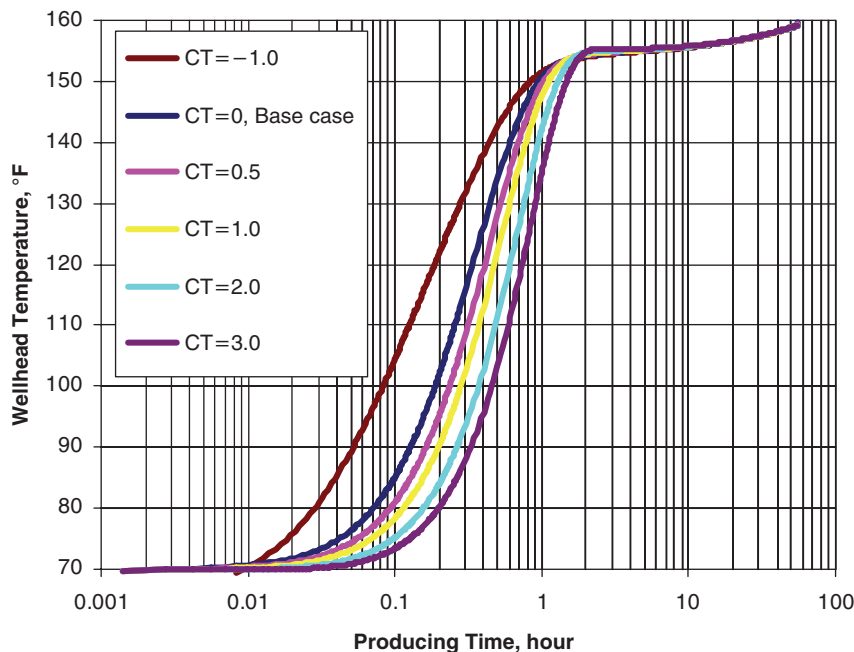


Fig. 19—Change of wellhead temperature with C_T vs. producing time.

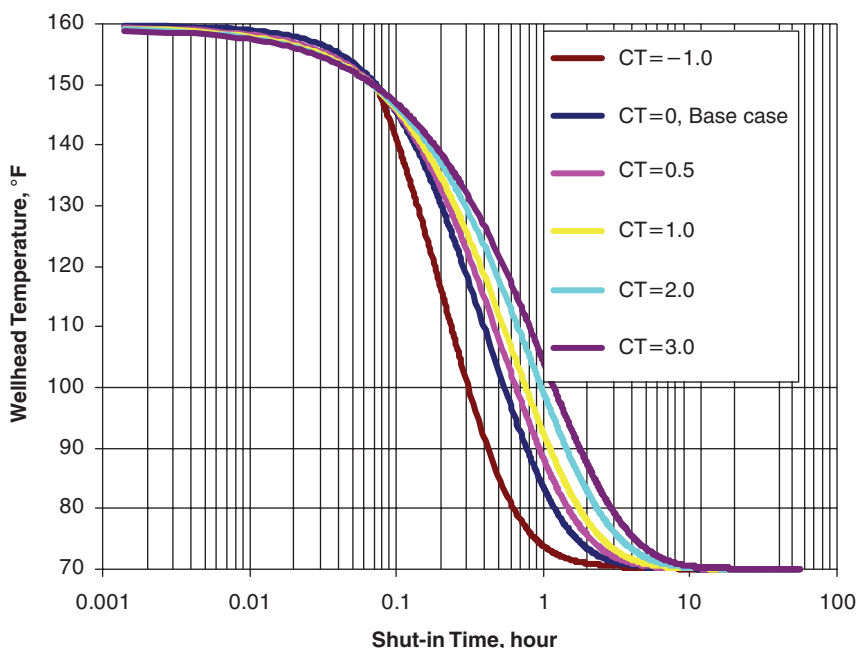


Fig. 20—Change of wellhead temperature with C_T vs. shut-in time.

sure DD for all cases is nearly the same (approximately 32%), and the derivative curves are shown in **Figs. 25 and 26** for the DD and BU tests, respectively. If the radius of the wellbore is decreased by a factor of r compared with the base case, the wellbore volume decreases exactly by r^2 , and the gas velocity and frictional loss inside the wellbore increase approximately by a factor of r^2 and r^5 , respectively. As both figures show, a higher wellbore volume gives higher wellbore storage, which delays the presence of true transient periods. Additionally, the figures indicate that as the wellbore volume decreases, the variable storage coefficient is more evident. Both figures also show that as the wellbore volume reduces, the temperature effects happen earlier because of less heat content of the tubing fluid. For instance, once the wellbore is shut in, the wellbore with the smallest tubing radius loses heat content more rapidly and thus the hump caused by the temperature effect shifts toward

the left of Fig. 26. The same statement can be made for Fig. 25 for the DD period.

Composite-Reservoir Case. To model a composite reservoir and investigate how temperature affects the transient pressure analysis which may lead to misdiagnosis, a few changes are made on the input data of the base case. The reservoir area is increased to 300 acres; up to the radius of 270 ft, the reservoir permeability is set to 100 md; from 270 ft to the outer reservoir boundary (at 2,040 ft), the permeability is set to 10 md. The DD and BU tests are run each for 138.889 hours. **Fig. 27** presents the comparison of pressure and derivative curves vs. pseudotime for two cases of the numerical isothermal and analytical models. According to this graph, the two models have a good agreement with each other, except at the initial time because of the assumption of a constant wellbore-storage

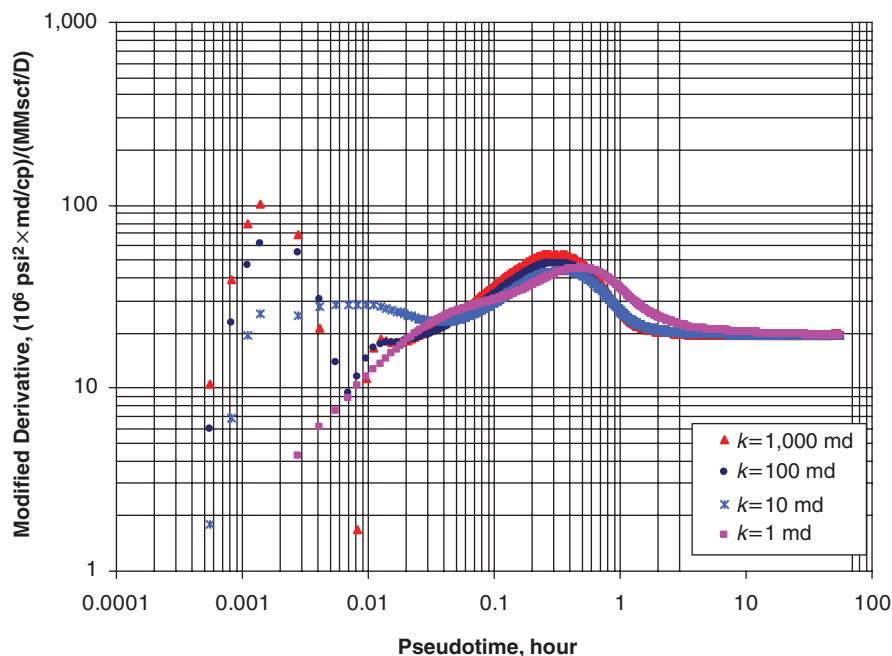


Fig. 21—Comparison of modified-derivative curves for different permeability values (DD test).

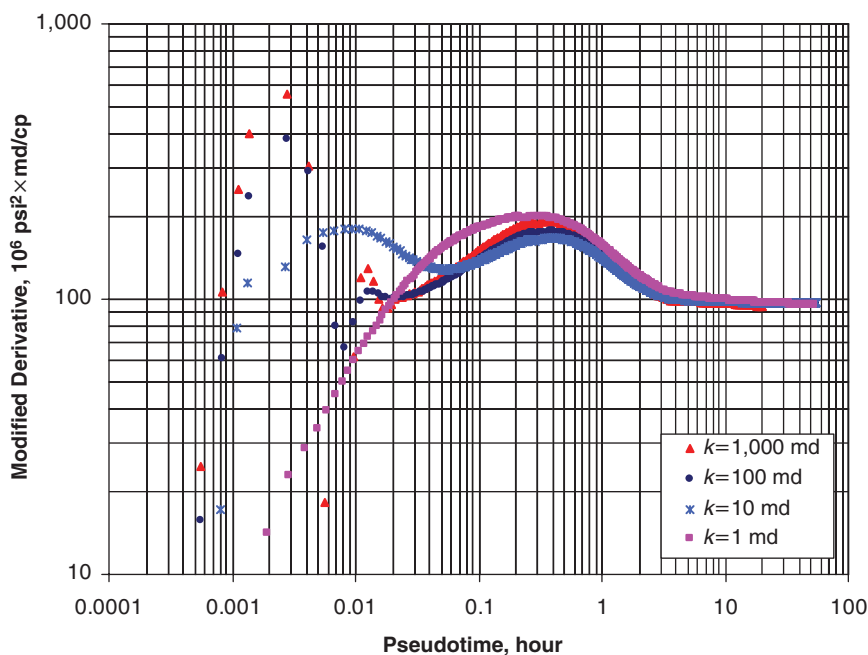


Fig. 22—Comparison of modified-derivative curves for different permeability values (BU test).

coefficient made in the analytical model. After this initial time, we can see the first transient regime (the first flat derivative curve), then the transition period, the second transient regime, and finally, a 45°-angle straight line that shows the pseudosteady-state period from which the reservoir size can be estimated. The two flat portions of the derivative curves and the straight line result in good estimation of the reservoir permeability (close to 98.6 and 10.05 md) and size ($3.90 \times 10^8 \text{ ft}^3$). In Fig. 28, the same functions shown in Fig. 27 have been compared, but this time between the numerical isothermal and nonisothermal models. As can be seen, the early time and transition period do not match each other because of the difference between the behaviour of the variable wellbore-storage coefficient (Fig. 17) and temperature effects. The nonisothermal simulator totally loses the first transient region as compared with

the isothermal simulator and instead shows a false transient region in the transition regime. If this false transient region is used to estimate the inner-cylindrical reservoir permeability where the actual permeability is 100 md, an incorrect value of 30 md will be obtained. Fig. 29 compares the behaviour of the derivative and primary-pressure-derivative (PPD) curves for the BU test of the numerical isothermal and nonisothermal simulators. For the BU test of any reservoir with any complexity, the PPD must be a constant or decreasing value; otherwise, it shows other nonreservoir phenomena (Mattar and Zaoral 1992). In the early time (less than 0.002 hours) of Fig. 29, the PPD increases, showing the wellbore effects. In this graph, the nonisothermal model again misses the first transient regime and directly falls in the transition period. The last sharp decreasing portion of the derivative curves is a result of

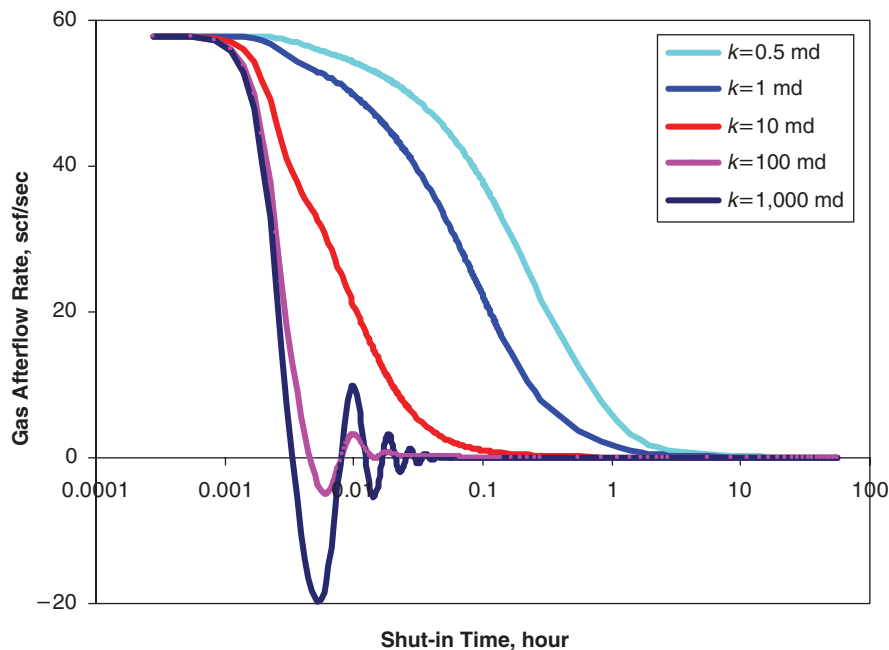


Fig. 23—Comparison of afterflow rates for different permeability values (isothermal case).

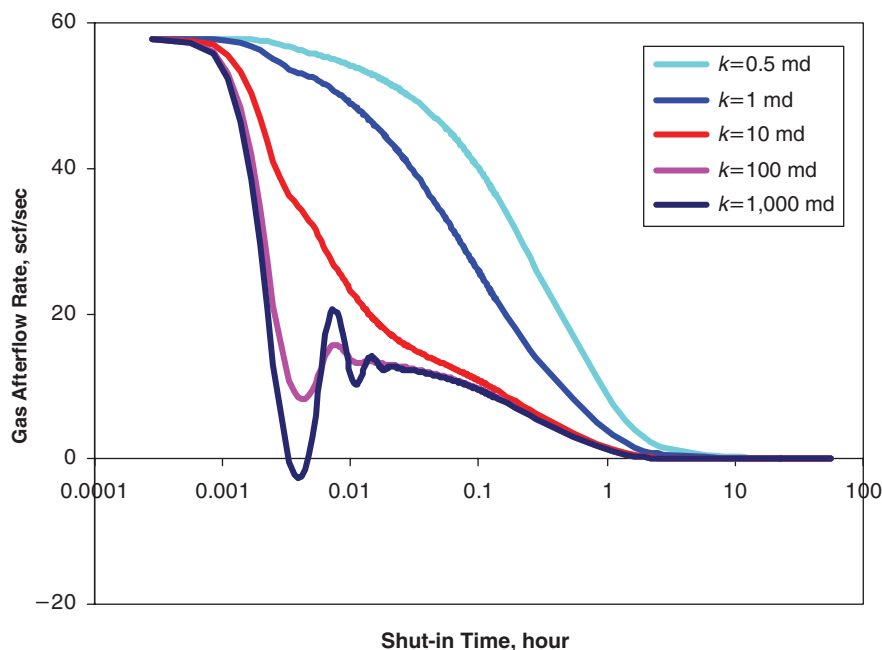


Fig. 24—Comparison of afterflow rates for different permeability values (nonisothermal case).

the no-flow boundary effect. This simple example shows how the interpretation of a simple reservoir can be misdiagnosed through nonisothermal effects. A nonisothermal coupled wellbore/reservoir simulator can help engineers prevent these kinds of errors in the real world.

The behaviour of gas-well testing when the wellbore is shut in at the wellhead has been investigated in this paper. As has been seen from the result of temperature effects in addition to wellbore dynamics, the behaviour and interpretation of nonisothermal gas reservoir well testing are quite different than isothermal ones. Special consideration must be taken into account to prevent a bad design and incorrect interpretation of the well test for such reservoirs. In this paper, only the well-testing applications of the developed (isothermal and nonisothermal) simulators have been studied. However, it is expected that these simulators have numerous other applica-

tions in studying flow-assurance issues, correction of gauge readings with respect to depth, designing and maintaining flowlines and production facilities, estimation of temperature distribution around the wellbore for well-logging applications, and so other issues.

Conclusions

The developed numerical (isothermal and nonisothermal) simulators have been used to study wellbore dynamics, particularly the momentum, mass (variable wellbore storage), and heat (forced convection inside tubing and heat loss from tubing to the surrounding medium) effects on the pressure-transient analysis. The main conclusions from this study can be summarized as follows:

1. A base case representing the well test in a deep HP/HT gas reservoir has been defined and thoroughly analyzed in terms of the behaviour of the pressure, temperature, gas density, gas velocity, and

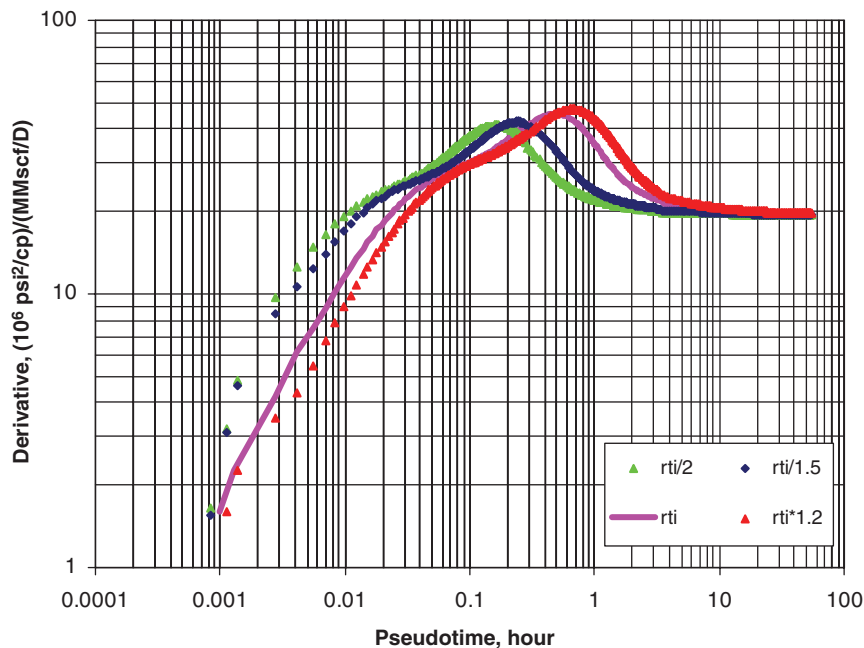


Fig. 25—Comparison of derivative curves for different r_{ti} (DD test).

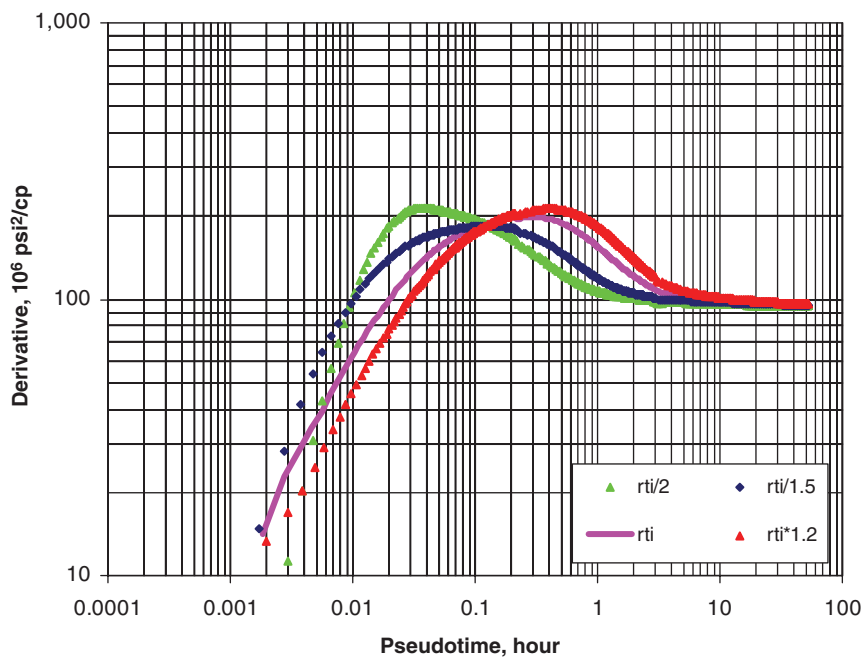


Fig. 26—Comparison of derivative curves for different r_{ti} (BU test).

overall heat-transfer coefficient in the wellbore. The behaviour of the derivative curves, sandface-flow rate, and wellbore-storage coefficient has been compared for both the DD and BU tests of the developed numerical isothermal and nonisothermal simulators. Whenever it is beneficial, these parameters have been also compared between the numerical and analytical models. It is concluded that the temperature effect increases the value of the wellbore-storage coefficient and thus extends the time of an afterflow rate compared with the case in which the temperature effects are ignored. In general, in a DD test of isothermal reservoirs where the well is shut in at the wellhead, the wellbore-storage coefficient shows an increasing trend. This increase occurs as a result of a decrease in the wellbore pressure caused by production that creates an increase in gas compressibility and thus increases the value of the wellbore-storage coefficient.

However, during the DD test of nonisothermal reservoirs and caused by hot-gas convection inside the tubing followed by heat loss from the tubing fluid toward the surrounding medium at early production time, a hump is seen in the behaviour of the wellbore-storage coefficient. After these two mechanisms, the pressure-drop mechanism takes over and therefore, after a few hours, the trend of increase in the wellbore-storage coefficient becomes similar to that of an increase in the wellbore-storage coefficient of the isothermal reservoirs. Similar behaviour can be seen during the BU test, but with a decreasing wellbore-storage coefficient trend as a result of the pressure increase inside the wellbore and consequently the decrease in the gas compressibility. In the BU period, the forced heat convection continues for a short period of time, and then the heat loss to the surrounding cold medium becomes the dominant heat-transfer mechanism.

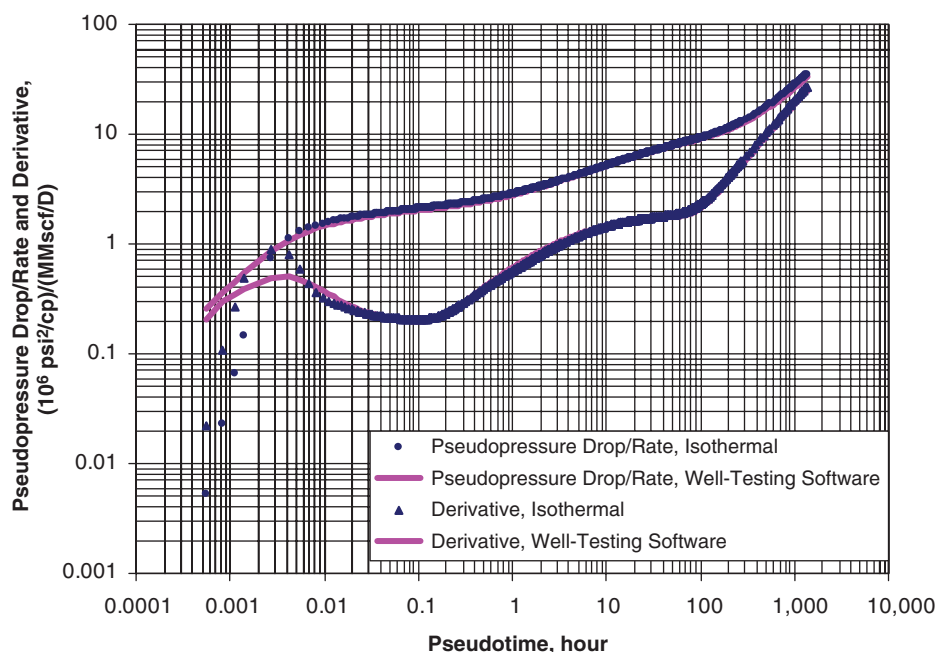


Fig. 27—Comparison of pseudopressure drop per rate and derivative curves for numerical isothermal model and analytical models (DD test).

2. It has been shown that the heat capacity of tubular and cement material should be considered in the modelling of nonisothermal coupled wellbore/reservoir systems by means of the thermal-storage parameter. This parameter has a large effect on the correct estimation of wellhead temperature.

3. The derivative curves and afterflow rates for a variety of permeabilities have been investigated. A distinct behaviour has been seen for the case of high-permeability reservoirs because of a large momentum effect. For instance, for a high-permeability reservoir, large backflow of gas from the wellbore toward the reservoir has been seen during shut-in time. This backflow is severe in the isothermal case compared with the nonisothermal case, and the after-flow effect lasts longer for the nonisothermal case compared with the isothermal case.

4. As the tubing internal radius is increased, the wellbore volume and thus the wellbore-storage effect increases. This delays the start of a real transient period in the derivative plots. Increasing the tubing internal radius considerably reduces the fluid velocity and also significantly decreases the frictional pressure drop inside the wellbore. This affects heat transfer inside the tubing and heat loss from the wellbore and thus the behaviour of the derivative curves.

5. In most cases studied in this paper, if the thermal effects are not recognized properly, the obtained plots may become misleading or a test may be designed improperly. In the case of using the analytical models, a simple nonisothermal gas reservoir may be mistakenly considered as a complex reservoir containing a single complexity or a combination of complexities (e.g., dual-porosity, multilayer, and/or composite reservoirs). A specific example for a composite reservoir has been provided that shows how the temperature effects may result in incorrect permeability estimation and distort the normal behaviour of the derivative curves. A numerical nonisothermal coupled wellbore/reservoir simulator (e.g., the one developed here) can overcome the deficiencies that exist in analytical models.

Nomenclature

- B_g = gas formation volume factor, bbl/scf
 c_t = total compressibility, 1/psia
 c_{ti} = total compressibility at initial reservoir condition, 1/psia
 C_T = thermal-storage parameter, dimensionless
 $C(t)$ = variable wellbore-storage coefficient, bbl/psia

- m = pseudopressure, psia
 N_{res} = number of radial grids in the reservoir, dimensionless
 N_{seg} = number of axial grids in the wellbore, dimensionless
 p = pressure, psia
 p_{wf} = bottomhole well flowing pressure, psia
 p_{ws} = bottomhole well shut-in pressure, psia
 PPD = primary pressure derivative, $(10^6 \text{ psi}^2/\text{cp})/\text{hr}$
 q_{sf} = sandface volumetric gas-flow rate, cf/sec
 q_{sfsc} = sandface volumetric gas-flow rate at standard condition, scf/sec
 q_{wh} = wellhead volumetric gas-flow rate, cf/sec
 q_{whsc} = wellhead volumetric gas-flow rate at standard condition, scf/sec
 t = time, seconds (hours)
 t_a = pseudotime, seconds (hours)
 T_{ci} = casing inside temperature, °F
 T_{co} = casing outside temperature, °F
 T_e = formation temperature, °F
 T_{ewb} = cementing/formation interface temperature (wellbore temperature), °F
 T_f = temperature of fluid inside tubing, °F
 T_{ti} = tubing inside temperature, °F
 T_{to} = tubing outside temperature, °F
 U_{to} = overall heat-transfer coefficient, Btu/(sec-ft²-°F)
 z = gas z-factor, dimensionless
 μ_g = gas viscosity, cp
 μ_{gi} = gas viscosity at initial reservoir condition, cp

Subscripts

- sc = standard condition(s)

Acknowledgements

The authors would like to thank the Alberta Ingenuity (now part of Alberta Innovates—Technology Futures), Natural Sciences and Engineering Research Council of Canada (NSERC), and the NSERC/Alberta Energy Research Institute (AERI)/iCORE/Foundation CMG Chair Funds for funding this research project.

References

- Agarwal, R.A. 1979. "Real Gas Pseudo-Time"—A New Function for Pressure Buildup Analysis of MHF Gas Wells. Paper SPE 8279 presented at

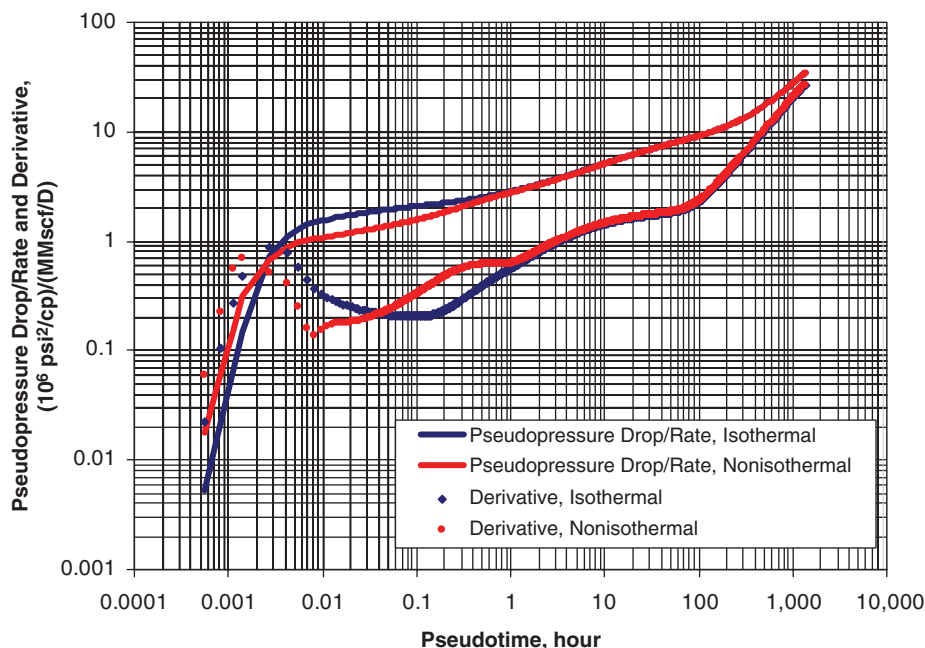


Fig. 28—Comparison of pseudopressure drop per rate and derivative curves for numerical isothermal and nonisothermal models (DD test).

- the SPE Annual Technical Conference and Exhibition, Las Vegas, Nevada, USA, 23–26 September. <http://dx.doi.org/10.2118/8279-MS>.
- Agarwal, R.G., Al-Hussainy, R., and Ramey, H.J. Jr. 1970. An Investigation of Wellbore Storage and Skin Effect in Unsteady Liquid Flow: I. Analytical Treatment. *SPE J.* **10** (3): 279–290; *Trans.*, AIME, **249**. SPE-2466-PA. <http://dx.doi.org/10.2118/2466-PA>.
- Al-Hussainy, R., Ramey, H.J. Jr., and Crawford, P.B. 1966. The Flow of Real Gases Through Porous Media. *J Pet Technol* **18** (5): 624–636; *Trans.*, AIME, **237**. SPE-1243-A-PA. <http://dx.doi.org/10.2118/1243-A-PA>.
- Bahonar, M., Azaiez, J., and Chen, Z. 2010. A Semi-Unsteady-State Wellbore Steam/Water Flow Model for Prediction of Sandface Conditions in Steam Injection Wells. *J Can Pet Technol* **49** (9): 13–21. SPE-140663-PA. <http://dx.doi.org/10.2118/140663-PA>.
- Bahonar, M., Azaiez, J., and Chen, Z. 2011a. Two Issues in Wellbore Heat Flow Modeling Along With the Prediction of Casing Temperature in the Steam Injection Wells. *J Can Pet Technol* **50** (1): 43–63. SPE-137134-PA. <http://dx.doi.org/10.2118/137134-PA>.
- Bahonar, M., Azaiez, J., and Chen, Z. 2011b. Transient Non-isothermal Fully Coupled Wellbore/Reservoir Model for Gas Well Testing, Part 1: Model Development. *J Can Pet Technol* **50** (9/10). SPE-149618-PA. <http://dx.doi.org/149618-PA>.
- F.A.S.T. WellTest, Version 7.1.2.6. 2009. Calgary, Alberta: Fekete Associates Inc.
- Fair, W.B. Jr. 1981. Pressure Buildup Analysis With Wellbore Phase Redistribution. *SPE J.* **21** (2): 259–270. SPE-8206-PA. <http://dx.doi.org/10.2118/8206-PA>.
- Fan, L., Lee, W.J., and Spivey, J.P. 1999. Thermal Effects on Gas Well Pressure Buildup Tests: Field Application. Paper SPE 55645 presented at the SPE Rocky Mountain Regional Meeting, Gillette, Wyoming, USA, 15–18 May. <http://dx.doi.org/10.2118/55645-MS>.
- Fan, L., Lee, W.J., and Spivey, J.P. 2000. Semi-Analytical Model for Thermal Effect on Gas Well Pressure-Buildup Tests. *SPE Res Eval & Eng* **3** (6): 480–491. SPE-68020-PA. <http://dx.doi.org/10.2118/68020-PA>.
- Hasan, A.R. and Kabir, C.S. 2002. *Fluid Flow and Heat Transfer in Wellbores*. Richardson, Texas: Textbook Series, SPE.
- Hasan, A.R., Kabir, C.S., and Lin, D. 2005. Analytic Wellbore-Temperature Model for Transient Gas-Well Testing. *SPE Res Eval & Eng* **8** (1): 240–247. SPE-84288-PA. <http://dx.doi.org/10.2118/84288-PA>.
- Hawkes, R.V., Su, Z., and Leech, D. 2001. Field Data Demonstrate Thermal Effects Important in Gas Well Pressure Buildup Tests. *J Can Pet Technol* **40** (11): 54–60. JCPT Paper No. 01-11-04. <http://dx.doi.org/10.2118/01-11-04>.
- Izgec, B., Kabir, C.S., Zhu, D., and Hasan, A.R. 2007. Transient Fluid and Heat Flow Modeling in Coupled Wellbore/Reservoir Systems. *SPE Res Eval & Eng* **10** (3): 294–301. SPE-102070-PA. <http://dx.doi.org/10.2118/102070-PA>.
- Kabir, C.S., Hasan, A.R., Jordan, D.L., and Wang, X. 1996. A Wellbore/Reservoir Simulator for Testing Gas Wells in High-Temperature Reservoirs. *SPE Form Eval* **11** (2): 128–134. SPE-28402-PA. <http://dx.doi.org/10.2118/28402-PA>.
- Mattar, L. and Santo, M. 1992. How Wellbore Dynamics Affect Pressure Transient Analysis. *J Can Pet Technol* **31** (2): 32–40. JCPT Paper No. 92-02-03. <http://dx.doi.org/10.2118/92-02-03>.
- Mattar, L. and Zaoral, K. 1992. The Primary Pressure Derivative (PPD)—A New Diagnostic Tool in Well Test Interpretation. *J Can Pet Technol* **31** (4): 63–70. JCPT Paper No. 92-04-06. <http://dx.doi.org/10.2118/92-04-06>.
- Meunier, D.F., Wittmann, M.J., and Stewart, G. 1985. Interpretation of Pressure Buildup Test Using In-Situ Measurements of Afterflow. *J Pet Technol* **37** (1): 143–152. SPE-11463-PA. <http://dx.doi.org/10.2118/11463-PA>.
- Sabet, M.A. 1991. *Well Test Analysis*, Vol. 8. Houston, Texas: Contributions in Petroleum Geology and Engineering, Gulf Publishing Company.
- Wang, X. 1996. Modeling Coupled Transient Transport of Mass, Momentum and Energy in Wellbore/Reservoir Systems. PhD Dissertation, The University of North Dakota, Grand Forks, North Dakota.

SI Metric Conversion Factors

acre	× 4.046 856	E+03 = m ²
bbl	× 1.589 873	E−01 = m ³
Btu	× 1.055 056	E+00 = kJ
Btu/lbm	× 2.326	E+03 = J/kg
Btu/(lbm·°F)	× 4.186 8*	E+03 = J/(kg·K)
Btu/(sec·ft·°F)	× 6.230 646	E+03 = W/(m·K)
Btu/(sec·ft ² ·°F)	× 2.044 175	E+04 = W/(m ² ·K)
cp	× 1.*	E−03 = Pa·s
°F	(°F−32)/1.8	= °C
°F/ft	× 1.822 678	E+00 = K/m
ft	× 3.048*	E−01 = m
ft/sec	× 3.048*	E−01 = m/s
ft ²	× 9.290 304*	E−02 = m ²
ft ³	× 2.831 685*	E−02 = m ³
ft ³ /D	× 2.831 685*	E−02 = m ³ /d
lbf	× 4.44 822	E+00 = N
lbm	× 4.535 924	E−01 = kg

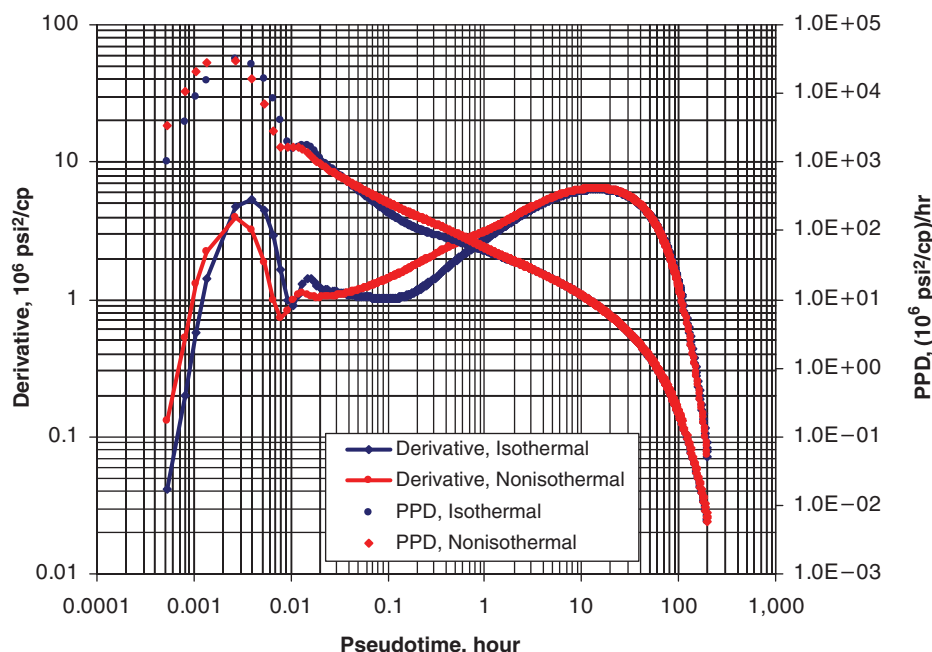


Fig. 29—Comparison of derivative and PPD curves for isothermal and nonisothermal models (BU test).

lbm/ft ³ × 1.601 846	E+01 = kg/m ³
md × 9.869 233	E-04 = μm ²
psia × 6.894 757	E+00 = kPa
psia ⁻¹ × 1.450 377	E-04 = Pa ⁻¹
psia/ft × 2.262 059	E+01 = kPa/m
scf/D × 2.863 640	E-02 = std m ³ /d

*Conversion factor is exact.

Appendix A

Definition of Pseudopressure, Pseudotime, Derivative, and PPD. *Pseudopressure.* The liquid-flow solution in the well-test analysis can be applied to the well-test analysis of gas reservoirs provided that pseudopressure and pseudotime functions are used instead of pressure and time, respectively. These functions were defined many years ago and will be described.

The gas pseudopressure was defined by Al-Hussainy et al. (1966), which takes care of dependence of the gas viscosity and compressibility on the pressure as

$$m(p) = 2 \int_0^p \frac{p dp}{\mu_g \times z}, \quad \text{..... (A-1)}$$

which has a unit of psi²/cp. During the DD, the drop in this quantity is divided by the gas-flow rate [i.e., $\Delta m(p)/q$] and is plotted on the y-axis (Fig. 28), which will have a unit of psi²/(cp × MMscf/D).

Pseudotime. The concept of pseudotime was introduced by Agarwal (1979) and was later modified. This function is defined as

$$t_a(t) = \mu_{gi} \times c_{ti} \int_0^t \frac{dt}{\mu_g \times c_i}, \quad \text{..... (A-2)}$$

where the gas viscosity and compressibility inside the integral are estimated at the average reservoir pressure during the DD and at the wellbore BHP during the BU. This pseudotime has a unit of hour on the basis of this equation.

Derivative. The derivative is defined as the slope of the semilog plot of pressure data vs. time and is given by

$$\text{Derivative} = \frac{d\Delta(m(p))}{d \ln(\Delta t)}, \quad \text{..... (A-3)}$$

As can be seen from this equation, the derivative has the same unit as the pseudopressure (i.e., psi²/cp) during the BU and is modified by dividing by the gas-flow rate during DD and thus will have a unit of psi²/(cp × MMscf/D).

PPD. The PPD for gas reservoirs is defined as

$$\text{PPD} = \frac{d\Delta(m(p))}{d\Delta t}, \quad \text{..... (A-4)}$$

which has the same unit as the pseudopressure but is divided by time. Therefore, the PPD has a unit of psi²/(cp × hour).

Authors



Mehdi Bahonar is a petroleum engineering PhD candidate who joined the Department of Chemical and Petroleum Engineering at the University of Calgary in September 2007 and is currently working at ConocoPhillips Canada as a reservoir engineering intern. He has received several academic awards, scholarships, and bursaries (including the Alberta Ingenuity PhD Graduate Student Scholarship) and authored or coauthored a number

of technical and journal papers. Bahonar has conducted research on topics related to steam injection in a fractured heavy-oil carbonate reservoir in Iran, natural convection and thermal radiation in the wellbore annulus, and modelling of transient nonisothermal fluid flow and heat transfer in coupled wellbore/reservoir systems. He holds a BSc degree in petroleum production engineering from the Petroleum University of Technology (PUT) in Iran and dual MSc/ MEng degrees in reservoir engineering from the University of Calgary/PUT, both as the first top student. He is a member of SPE and the Association of Professional Engineers, Geologists, and Geophysicists of Alberta.



Jalel Azaiez is currently a professor in the Department of Chemical and Petroleum Engineering at the University of Calgary. His expertise is in the field of mathematical modelling and numerical simulation of fluid flows, with a particular focus on complex systems. These include non-Newtonian-fluid flows, rheological modelling of fibre and polymer systems, viscous fingering, and other chemically or thermally driven instabilities in porous media. Azaiez has published more than 40 refereed journal papers, has published more than 20 refereed conference proceedings papers, and has delivered 55 conference talks. He has also presented nine invited talks and seminars worldwide. Azaiez holds a Diplôme d'Ingénieur from the École Centrale de Paris in France and MSc and PhD degrees from Stanford University.

ities in porous media. Azaiez has published more than 40 refereed journal papers, has published more than 20 refereed conference proceedings papers, and has delivered 55 conference talks. He has also presented nine invited talks and seminars worldwide. Azaiez holds a Diplôme d'Ingénieur from the École Centrale de Paris in France and MSc and PhD degrees from Stanford University.



Zhangxing (John) Chen is currently a professor at the University of Calgary, is Director of iCentre Simulation and Visualization, and holds the NSERC/AERI/Foundation CMG Senior Research Chair in reservoir simulation and iCORE Industrial Chair in reservoir modelling. He formerly held a Tengfei Chaired and Chang Jiang Chaired Professorship at Xi'an Jiaotong University, Tepin Professorship of Energy

and Resources at Peking University, Ziqiang Professorship at Shanghai University, and Gerald J. Ford Research Professorship at Southern Methodist University. Chen holds a BS degree from the University of Jiangxi (China), an MS degree from Xi'an Jiaotong University (China), and a PhD degree from Purdue University, USA.